International Journal of Chemical, Materials and Biomolecular Sciences
ISSN: 2415-6620
Vol:5, No:1, 2011

Heat Transfer, Fluid Flow, and Metallurgical Transformations in Arc Welding: Application to 16MND5 Steel

F. Roger, A. Traidia, B.Reynier

***Abstract*—** Arc welding creates a weld pool to realize continuity between pieces of assembly. The thermal history of the weld is dependent on heat transfer and fluid flow in the weld pool. The metallurgical transformation during welding and cooling are modeled in the literature only at solid state neglecting the fluid flow. In the present paper we associate a heat transfer – fluid flow and metallurgical model for the 16MnD5 steel. The metallurgical transformation model is based on Leblond model for the diffusion kinetics and on the Koistinen-Marburger equation for Marteniste transformation. The predicted thermal history and metallurgical transformations are compared to a simulation without fluid phase. This comparison shows the great importance of the fluid flow modeling.

***Keywords*—** Arc welding, Weld pool, Fluid flow, Metallurgical transformations.

I. Introduction

GAS Tungsten arc welding process (GTAW) realizes metallic continuity by fusion of assembly. The resulting weld area is characterized by a fusion zone and a heat affected zone where solid-solid metallurgical transformations take place during welding and cooling steps.

Considering metallurgical transformations in welding simulation is necessary because they influence residual stresses and distortions. Indeed, thermal and mechanical material properties are fraction of phase dependent: for example thermal expansion coefficient of Austenite is equal to 23.5e-6 $°C^{-1}$ while its value is 15e-6$°C^{-1}$ for Ferrite [1]. Moreover, for steel like 16MND5 (A508 Cl3), inelastic strains like Transformation Induced Plasticity result of phases transformation under mechanical stresses.

Modeling of metallurgical transformation during welding or heat treatment has been extensively studied [2]-[5], [8]. In these previous works, phase change takes place at solid state between room temperature and austenitization temperature (1200°K). The cooling conditions are described using CCT diagram. In welding, fusion and fluid flow in the weld pool lead to quite different thermal histories because of the convective heat transfer in the weld pool. The heating and cooling speed are very high, several hundreds of degree per second. Therefore to predict the metallurgical transformations during welding, we consider the fluid flow in the weld pool to have realistic heating and cooling conditions.

A heat transfer, fluid flow and metallurgical transformation model have been developed. The weld pool is considered as an incompressible and viscous fluid governed by Navier-Stokes equation. Solid metallurgical transformations are based on a 16MnD5 steel CCT diagram and metallurgical kinetics are based on Leblond model [2] for diffusion equations. Martensite evolution is described by Koistinen Marburger equation [6] with a minimum cooling speed condition. Koistinen-Marburger equation coefficients have been adjusted to CCT diagram with a bainite phase fraction dependence. Metallurgical predictions will be compared to a thermo-metallurgical simulation without fluid phase.

II. Mathematical Formulation of the Problem

The model is divided into two parts. The first one is a heat transfer and fluid flow simulation. The second part evaluate fraction of each metallurgical phase from the thermal history given by the previous model.

A. Heat transfer and fluid flow in the weld pool

In arc welding, arc heats the top surface of the assembly during a few seconds to create a weld pool. This surface heat source can be approximate by a Gaussian heat distribution according the following equation:

$$q_{welding} = \frac{3\eta UI}{\pi r_a^2}\exp(-3\frac{r^2}{r_a^2}) \quad (1)$$

F. Roger. is an Assistant Professor with Mechanical Engineering Laboratory, Ecole Nationale Supérieure de Techniques Avancées, Paristech, Chemin de la Hunière, Palaiseau 91120 FRANCE (corresponding author to provide phone: Tel: +33 169 319 815; fax: 00-33-169339906; e-mail: frederic.roger@ ensta-paristech.fr).

A. Traidia is with both: The Laboratory of Mechanics, Materials and Structures Group at Ecole Nationale Supérieure de Techniques Avancées, Chemin de la Hunière, 91120 Palaiseau Cedex, FRANCE (Tel: +33 169 319 815; e-mail: abderrazak.traidia@ensta-paristech.fr) & The Technical Center AREVA NP, BP 40001 SAINT MARCEL, 71328 Chalon Sur Saone Cedex, FRANCE.

B. Reynier. is an Associated Professor with Mechanical Engineering Laboratory, Ecole Nationale Supérieure de Techniques Avancées, Paristech, Chemin de la Hunière, Palaiseau 91120 France (e-mail: bertrand.reynier@ ensta-paristech.fr).

Where $q_{welding}$ is the surface heat flux ($W.m^{-2}$), U is the welding voltage (V), I is the current (A), η is the arc efficiency (0.68 for GTAW), r_a is the arc radius (m).

The other sides of the assembly are submitted to air convection. This heat distribution creates thermal gradient at the top surface. The surface tension of stainless steel is very sensitive to temperature. As a consequence, surface tension gradients occur. In the present study, we consider that the temperature coefficient of surface tension is temperature dependent with a constant sulfur content of 20 ppm. Generally, this coefficient is negative for pure metals but the presence of sulfur in stainless steel can make its value positive.

The following expression is used for the temperature coefficient of surface tension [7]:

$$\frac{\partial \gamma}{\partial T} = -A_\gamma - R_g \Gamma_S \ln\left(1 + Ka_S\right) - \frac{K(T)a_S}{1 + K(T)a_S}\frac{\Gamma_S \Delta H_0}{T} \quad (2)$$

$$K\left(T\right) = k_1 \exp\left(-\frac{\Delta H_0}{R_g T}\right) \quad (3)$$

Where γ is the surface tension, A_γ is a constant, R_g is gas constant, Γ_S is surface excess at saturation, a_s is activity of sulfur, ΔH_0 is standard heat of adsorption, k_1 is the entropy factor . The values of these parameters are presented in table 1 in appendix.

Gradients of surface tension at the top surface of the weld pool lead to shear stresses according to the Marangoni effect. This shear stress produces fluid flow in the weld pool as the liquid metal is viscous.

The Marangoni shear stress boundary condition, for an axial symmetric heating, is described by the following equation:

$$\mu \frac{\partial u}{\partial z} = f_l \frac{\partial \gamma}{\partial T}\frac{\partial T}{\partial r} \quad (4)$$

Where r is the radius from the arc center, z is the height, u is the radial velocity, μ is the dynamic viscosity, γ is the surface tension, f_l is the liquid fraction (equal 1 at the fluid free surface and decreasing from 1 to 0 for solid state in the mushy zone of the weld). The normal fluid velocity is set to zero.

The governing equation for the heat transfer and fluid flow are expressed as follows:

Conservation of mass:

$$\nabla.\vec{v} = 0 \quad (5)$$

Conservation of momentum:

$$\rho\left(\frac{\partial \vec{v}}{\partial t} + \vec{v}.\nabla\vec{v}\right) = -\nabla p + \mu\nabla.\left(\nabla\vec{v} + {}^t\nabla\vec{v}\right) + \vec{F}_b \quad (6)$$

Where $\vec{v}$ is the fluid velocity, $\vec{F}_b$ is the buoyancy force (Boussinesq approximation) and is expressed by :

$$\vec{F_b} = \rho_0(1 - \beta\left(T - T_{ref}\right)\vec{g} \quad (7)$$

Where ρ_0 is the density at $T=T_{ref}$, β is the thermal expansion coefficient.

Energy conservation:

$$\rho C_p \frac{\partial T}{\partial t} + \rho C_p \vec{v}.\nabla T = \nabla\left(\lambda\nabla T\right) + \rho L_f \frac{df_l}{dt} \quad (8)$$

Where f_l has been defined in the Marangoni equation (2), L_f is the latent heat of fusion. The main parameters for the heat and fluid flow simulation are presented in table 1.

B. Metallurgical transformations

Welding is associated to anisothermal metallurgical transformation with high heating and cooling speeds. In the case of 16MND5 steel, kinetics corresponds to diffusion and martensitic transformations. J.B. Leblond [2] uses fraction of each phase z_i as variable and proposes to describe all this kinetics using Ordinary Differential Equations (ODE). The Martensitic transformation is usually described by the Koistinen Marburger equation [6].

B.1 Leblond-Devaux's model

The evolution of fraction of phase is governed by temperature for Austenite, Ferrite-Perlite and by temperature and cooling rate for bainite. The Austenite grain size have also a great influence as it modify the Continuous Cooling Diagram of the steel. This parameter can be add as a variable in the coefficient of the transformation equations.

The general form of the evolution equation is the following ODE:

$$\dot{z} = \frac{z_{eq}(T) - z}{\tau(T)} \quad (9)$$

Where z_{eq} is the fraction of phase at the thermodynamics equilibrium for a constant temperature T, so that when $z=z_{eq}(T)$, the equation (9) doesn't evolve. τ is a characteristic time to reach $z=z_{eq}$ from $z=0$. The temperature dependence of z_{eq} is obtained at very low heating rates. For Martensite transformation, J.B. Leblond use the same ODE to keep the same framework but with a shorter characteristic time.

The figure 1 shows the qualitative predictions of equation 9.

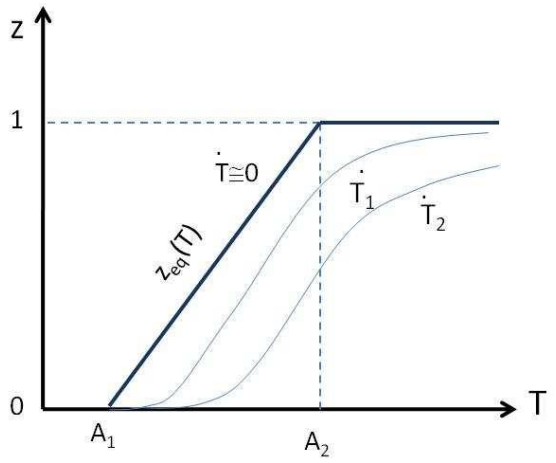

Fig. 1 Temperature dependence of z according to the heating rate. For very low heating rate, z(t) follows $z_{eq}[T(t)]$ [Leblond 1984]. $\dot{T} < \dot{T}_1 < \dot{T}_2$

At each time, the sum of all the fractions of phase is equal to 1. Then, $z_1+z_2+z_3+z_4=1$.

Where z_1 is fraction of ferrite-perlite, z_2 is fraction of bainite, z_3 is fraction martensite and z_4 is fraction of austenite.

This condition can be written in time derivative again :

$$\dot{z}_1+\dot{z}_2+\dot{z}_3+\dot{z}_4=0 \tag{10}$$

Leblond writes equation (9) again in a more suitable form for generalization, for a unique 1→2 transformation, equation (9) becomes :

$$\dot{z}_2=\frac{z_{eq}(T)-z_2}{\tau(T)}+\frac{z_{eq}(T)}{\tau(T)}z_1-\frac{z_{eq}(T)}{\tau(T)}z_1$$

$$=\frac{z_{eq}(T)}{\tau(T)}(1-z_1)-\frac{z_2}{\tau(T)}+\frac{z_{eq}(T)}{\tau(T)}z_1$$

$$\dot{z}_2=\frac{z_{eq}(T)}{\tau(T)}z_2-\frac{z_2}{\tau(T)}+\frac{z_{eq}(T)}{\tau(T)}z_1$$

$$=\frac{z_{eq}(T)}{\tau(T)}z_1-\frac{1-z_{eq}(T)}{\tau(T)}z_2$$

$$\dot{z}_2=k_{12}(T)z_1-l_{12}(T)z_2 \tag{11}$$

With $k_{12}(T)=\frac{z_{eq}(T)}{\tau(T)}$ and $l_{12}(T)=\frac{1-z_{eq}(T)}{\tau(T)}$

For a unique 1→2 transformation, the equation (10) gives:

$$\dot{z}_1=-\dot{z}_2=-k_{12}(T)z_1+l_{12}(T)z_2 \tag{12}$$

$$if\ k_{12}(T)z_1-l_{12}(T)z_2>0$$

For the 2→1 transformation, we have:

$$\dot{z}_1=k_{21}(T)z_2-l_{21}(T)z_1 \tag{13}$$

$$\dot{z}_2=-k_{21}(T)z_2+l_{21}(T)z_1 \tag{14}$$

$$if\ k_{21}(T)z_1-l_{12}(T)z_2>0$$

There is no transformation $\dot{z}_1=\dot{z}_2=0$ if

$k_{12}(T)z_1-l_{12}(T)z_2\le 0$ and $k_{12}(T)z_1-l_{12}(T)z_2\le 0$

For a good description of the Austenite/Bainite transformation which takes place in a wide range of cooling conditions, Leblond add a cooling rate dependence for the k_{42} and l_{42} functions and proposed the following factorized forms:

$$k_{42}(T,\dot{T})=f_{42}(T)*h_{42}(\dot{T}) \tag{15}$$

$$l_{42}(T,\dot{T})=g_{42}(T)*h_{42}(\dot{T}) \tag{16}$$

B.2 Martensite transformation

Martensite phase appears at very high cooling rates far from thermodynamic equilibrium. The phase change transformation is so quick (about the speed of sound in a metal) that we can consider it as instantaneous. That's why Koistinen and Marburger have developed a transformation equation for Martensite without time dependence. In the high cooling rate conditions, the Martensite fraction is dependent on the temperature shift related to the Martensite start temperature (Ms). The Koistinen-Marburger equation is as follow:

$$z_3=z_4*\left(1-\exp\left(\beta*[Ms-T]^+\right)\right) \tag{17}$$

Where $[.]^+$ is the positive part operator, Ms is the Martensite start temperature, β is a coefficient adjusted such that when T=Mf, $z_3=0.99*z_4$.

B.3. Metallurgical transformation in 16MnD5 steel

Leblond identify the fonctions k(T) and l(T) of the transformation equations using a CCT diagram for the 16MND5 steel (see Fig. 2). All the identified coefficients for the transformations are presented in table II.

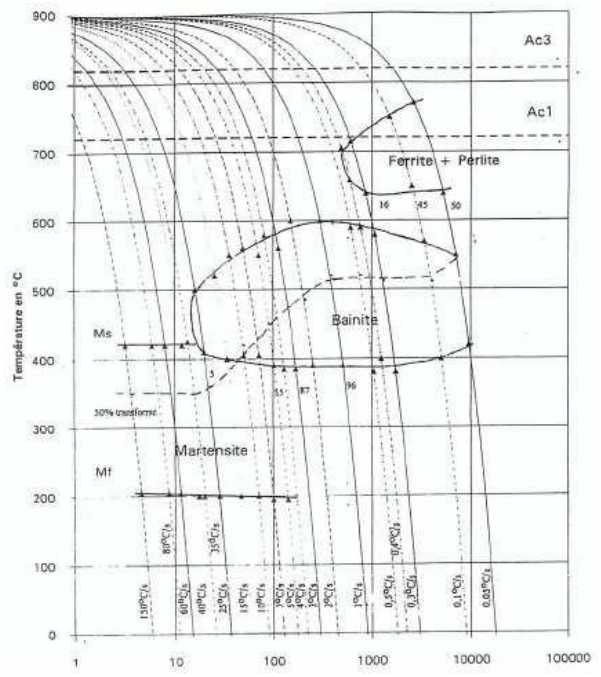

Fig. 2 CCT diagram for 16MnD5 steel [Martinez 1999] (austenite grain size : 9, austenitization time 5 min at 900°C)

For the Martensite transformation, we use the Koistinen Marburger equation with a Martensite start temperature dependent on the fraction of bainite z_2 formed before this temperature. Based on the CCT diagram, we choose the following dependence:

$$Ms(z_2) = Ms_0 - A * z_2 \tag{18}$$

From the CCT diagram, we fixed M_{S0} to 688°K and A to 45.5 As Martensite is formed at high cooling rate, we decide to add a cooling rate condition to the Koistinen-Marburger equation.

To detect the point of the welded structure where Martensite transformation takes place, we decide to add an ODE equation which evolves when the cooling rate is in the range of Martensite transformation. The ODE is the following one:

$$\dot{y} = \left[\dot{T} < \dot{T}_m\right] * [T < Ms(z_2)] \tag{19}$$

Where [cond.]=1 if the condition is realized and zero otherwise. $\dot{T}_m$ is the minimum cooling speed to form Martensite,. In the 16MND5 CCT diagram it corresponds to 1°C/s.

The resulting Martensite transformation equation is:

$$z_3 = z_4 * \left(1 - \exp\left(\beta(z_2) * \left[Ms(z_2) - T\right]^+\right)\right) * [y > 0] \tag{20}$$

The coefficient β is choosen dependent of the bainite fraction because the shift between Martensite start and Martensite finish temperature is not constant in the CCT diagram. We use the following formula:

$$\beta(z_2) = \frac{ln 0.01}{Ms(z_2) - Mf} \tag{21}$$

Where Martensite finish temperature is fixed to 473°K. The value 0.01 is fixed to have $\left(1 - \exp\left(\beta(z_2) * \left[Ms(z_2) - T\right]^+\right)\right) = 0.99$ i.e. when T is equal to Mf, 99% of Austenite is transformed into Martensite.

III. Application: Modeling of Spot Arc Welding

Previous Heat transfer, fluid flow and metallurgical transformations models have been applied to simulate the arc spot welding of a 16MnD5 steel disk (thickness 6 mm and radius 20mm). The arc heating is maintained constant during 5 seconds at the top center of the disk followed by air cooling during 15s. As heating and clamping conditions are axial symmetric, the simulation is done in 2D axial symmetric conditions. Simulations are realized using the finite element code Comsol Multiphysics©.

As metallurgical transformation kinetics equations are not present in the Comsol modules, we have developed our own toolbox using the Partial Differential Equation module.

The simulations of weld pool evolution and the metallurgical transformations are described in the next sections.

A Heat transfer and fluid flow in the weld pool

The following figure shows fluid flow and temperature field at the end of the heating time.

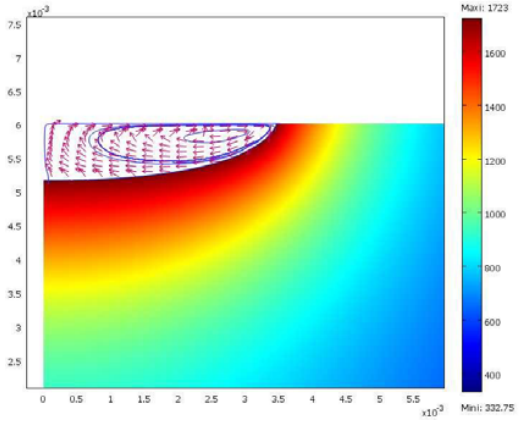

Fig. 3 Fluid flow in the weld pool (streamline and velocity) and temperature field in the solid zone at the end of heating (t=5s)

The Marangoni effect induced a clockwise vortex and then arc heat is convected from the center of the top surface to the radial direction. The resulting weld pool is wide (r=3.4mm) and weakly penetrated (0.8mm). The maximum radial velocity at the top surface is 0.18m/s near the outer edge of the weld pool.

The thermal history of vertical points at different height (0 to 6mm from the bottom of the disk) at r=0 is presented in figure 4.

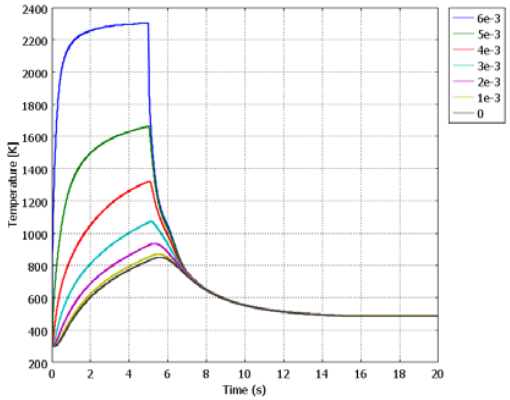

Fig. 4 Thermal history of vertical points at r=0 located at different height (0,1,2,3,4,5 and 6 mm)

The maximum cooling rate for these different height (0-1-2-3-4-5mm) is respectively from the bottom to the top (-110, -120,-145,-210,-340,-340,-540,-1300°K/s). Please note that the 6mm height point presents a singularity and is not considered.

B Metallurgical transformations in the welded zone

The simulation start with a cold disk having a fraction of ferrite-perlite z_1=0.4 and bainite z_2=0.6.

At the end of arc heating (t=5s) the austenitic phase distribution is presented in figure 5 (fraction of z_4). From this austenite phase, martensite and bainite will be formed during cooling. The Figure 6 shows the final Martensite phase distribution after cooling (t=20s).

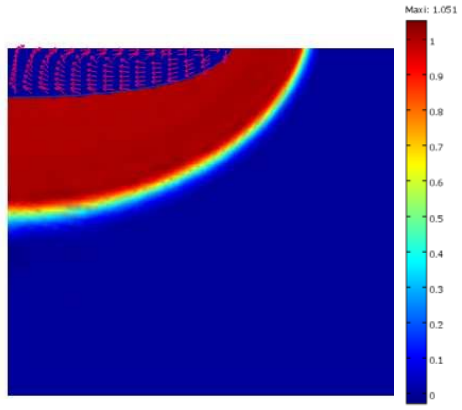

Fig. 5 : Austenite distribution and weld pool at the end of arc heating (t=5s)

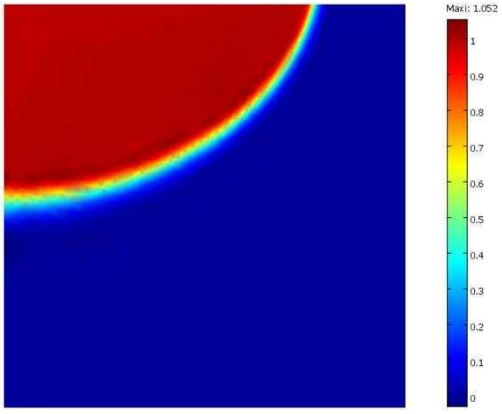

Fig. 6 : Martensite distribution after cooling (t=20s)

The phase fraction time evolutions for the top center point and a point located at the mid-height (r=0; z=3mm) are presented in figure 7 (a) (b).

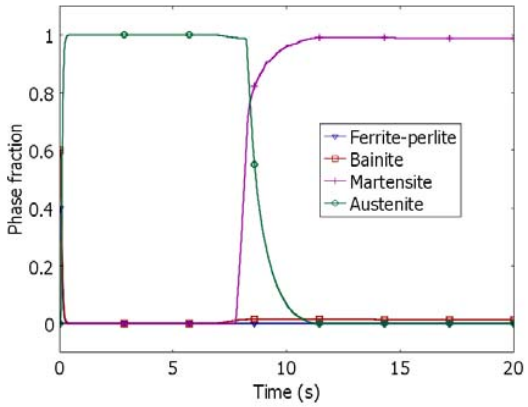

(a)

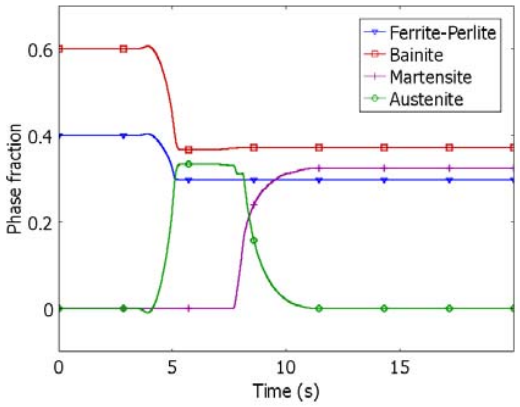

(b)

Fig. 7 : Phase fraction time evolutions for the top center point (a) and a point located at the mid- height (b)

Martensite is formed after cooling in the fusion zone with a little bit of Bainite (fig 7 a). In the heat affected zone, (fig 7b) we have a mixture of Bainite, Ferrite and Martensite. The sum of phase fractions is closed to 1 (equation 10), so this constraint is well respected in our model.

C Comparison with a thermo-metallurgical simulation

To study the importance of considering the weld pool in the modeling, we compare prediction with and without liquid phase. The weld pool, with convective heat transfer, increases the heat flow rate inside the workpiece. The thermal history of vertical points on the axis at different heights (0 to 6mm from the bottom of the disk) is shown in figure 8. It permits a comparison with the fully coupled model results (Fig 4).

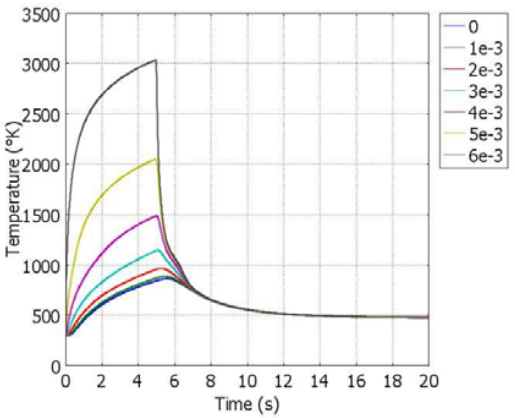

Fig. 8 : Thermal cycles at the center of the disk for different height.

In the case of pure conduction (without fluid), the maximum temperature in the weld pool is higher (3000°K) than in the previous model (2300°K). The phase fraction is very different when we neglect the fluid phase. Indeed, the figure 9 shows the phase evolution at a mid-height point (r=0mm, z=3mm). This evolution is quite different from those of Fig 7b.

The final phase is made of quite Martensite while it is a mixture of Bainite-Martensite and Ferrite for the fluid flow model.

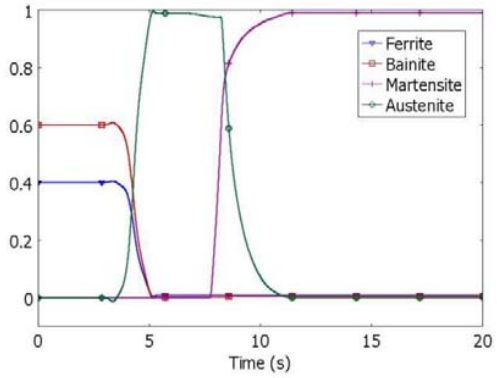

Fig. 9 : Phase fraction time evolutions for a point located at the middle height

IV. CONCLUSION

The prediction of metallurgical transformations in welding, which is controlled by the thermal history, necessitates considering the fluid flow modeling in the weld pool. Usually, the metallurgical consequences of welding are modeled using heat conduction model like in the commercial software Sysweld©.

APPENDIX

TABLE I
MATERIALS PROPERTIES USED IN SIMULATIONS

Symbol	Quantity	Conversion from Gaussian and CGS EMU to SI [a]
ρ	Density	6080 to 7272 kg.m^{-3}
c_p	Specific heat	510 to 796 J.kg^{-1}.K^{-1}
k	Thermal conductivity	37.7 to 26.9$W.m^{-1}.K^{-1}$
μ	Dynamic viscosity	0.05 kg.m^{-1}.s^{-1}
σ	Electrical conductivity	7.7 $\times 10^5$ Ω^{-1}.m^{-1}
T_l	Liquidus temperature	1723 K
T_s	Solidus temperature	1673 K
a_s	Sulfur activity	0.001 wt%
R_g	Gas constant	8314 J.kg^{-1}.mole^{-1}.K^{-1}
ΔH_0	Latent heat of fusion	-1.66 $\times$ 10^8 J.kg^{-1}.mole^{-1}
Γ_s	Surface excess of sulfur at saturation	1.3 $\times$ 10^{-8} J.kg^{-1}.mole^{-1}.m^{-2}
γ_m	Surface tension at pure metal	1.943 N.m^{-1}
k_1	Entropy factor	3.18 $\times$ 10^{-3} N.m^{-1}.K^{-1}
A_γ	Constant in surface tension gradient	4.3 $\times$ 10^{-4} N.m^{-1}.K^{-1}

TABLE II
PARAMETERS USED FOR THE COEFFICIENTS
OF FRACTION PHASE IN THE LEBLOND MODEL

Temp. °C	0	730	750	770	790	810
k_{14}	0	0	0.22	0.53	1.05	2.02
k_{24} (s^{-1})						
k_{34}						
l_{14}	1	1	0.97	0.94	0.87	0.76
l_{24} (s^{-1})						
l_{34}						
Temp. °C	830	840	860	880	900	1000
k_{14}	4.55	5.6	7.37	10.8	20	20
k_{24} (s^{-1})						
k_{34}						
l_{14}	0.45	0	0	0	0	0
l_{24} (s^{-1})						
l_{34}						

Ferritic-pearlitic transformation

Temp. °C	0	600	620	800	1000
k_{41} (s^{-1})	1e-4	1e-4	1.8e-3	0	0
l_{41} (s^{-1})	0	0	2e-4	2e-3	2e-3

Bainitic transformation

Temp. °C	0	340	350	450	550	1000
f_{42} (s^{-1})	0	0	0.014	0.067	0	0
g_{42} (s^{-1})	0	0	0	0	0.067	0.067

Cooling rate (°C.s^{-1})	-11.95	-4.16	-2	-0.416	-0.194	-0.0194
h_{42}	0.2	1	1.5	0.22	0.1	0.0044

REFERENCES

[1] Martinez, "Jonction 16MnD5-Inconel 690-316LN par soudage diffusion. Elaboration et calculs des contraintes résiduelles de procédé », PhD, Ecole Nationale Supérieure des Mines de Paris, 1999.
[2] J. B. Leblond, J.C. Devaux, "A new kinetic model for anisothermal metallurgical transformations in steels including effect of austenite grain size", Acta Mater, vol 32, p137-146, 1984.
[3] T. Inoue, Z.G Wang, "Coupling between stress, temperature and metallic structures during processes involving phase transformations", Mat. Sci. Technol., vol 19, p845-850, 1985.
[4] Z.G. Wang, T. Inoue, "Viscoplastic constitutive relation incorporating phase transformation – application to welding", Mat. Sci. Technol, vol 19, p899-903, 1985.
[5] F. Waeckel, "Une loi de comportement thermométallurgique des aciers pour le calcul mécanique des structures », PhD, ENSAM, 1984.
[6] D.P. Koistinen, R.E. Marburger, « A general equation prescribing extend of austenite-martensite transformation in pure Fe-C alloys and plain carbon steels", Acta Metall, vol 7, p59-60, 1959.
[7] A. Traidia, F. Roger, E. Guyot, "Optimal parameters for pulsed gas tungsten arc welding in partially and fully penetrated weld pools", Int. J. Therm. Sci., 49, p1197-1208, 2010.
[8] Z. Moumni, F. Roger, N.T. Trinh, "Theoretical and numerical modeling of the thermomechanical and metallurgical behavior of steel", Int. J. Plasticity, 2010.